Titanium Nitride Precipitation Behavior in Thin-Slab Cast High-Strength Low-Alloy Steels

MICHAEL T. NAGATA, JOHN G. SPEER, and DAVID K. MATLOCK

To assess the potential for obtaining and utilizing titanium nitride (TiN) refinement *via* the increased postsolidification cooling rates associated with thin-slab casting, TiN particle size distributions were evaluated by transmission electron microscope (TEM) examination of carbon extraction replicas. Eight commercially produced thin-slab cast TiN steels, nominally 0.05 pct C, 1.2 pct Mn, and one conventionally cast steel were received. Thin slab samples were taken from three locations in the production process: quenched after casting before the tunnel furnace, quenched after tunnel furnace soaking, and the as-rolled and air-cooled final product. Effects of cooling rate were evident in the results and agree with previously documented behavior, where precipitate size decreases with increased cooling rate. Statistical differences in particle size between specimens from steels with different chemistries were shown. These variations result from differences in the driving force for precipitation, rates of coarsening, and differences in volume fraction due to changes in steel composition. The interaction of composition and processing, such as soaking in the tunnel furnace and rolling, was found to be important. For example, the hyperstoichiometric steel (excess Ti) exhibited fine TiN after casting and soaking, but dramatic coarsening after hot rolling. This behavior was attributed to deformation enhanced particle coarsening, or incomplete precipitation after soaking, followed by continued growth during subsequent processing.

I. INTRODUCTION

THIN-SLAB casting is being used increasingly as a means of producing sheet steels because of its reduced capital costs. While initial difficulties due to differences in production methods have been overcome and a viable product is being produced, much remains unknown about this relatively new technology. Some metallurgical factors associated with thin-slab casting, when compared to conventional casting, include faster postsolidification cooling rates, less time at very high temperatures, predominance of direct charging, and lower slab soaking temperatures. These intrinsic differences may provide an opportunity to control microstructure and properties in new ways through processing and chemistry.

One aspect of special interest is the precipitation behavior of microalloy carbides and nitrides. For example, there may be potential for obtaining and utilizing titanium nitride (TiN) refinement *via* the increased postsolidification cooling rates[1] associated with thin-slab casting. The differences between conventional casting and thin-slab casting may conceivably change the precipitation and coarsening behavior of TiN precipitates leading to a finer precipitate dispersion. Smaller precipitates are beneficial in retarding austenite grain growth, according to the Gladman equation:

$$R = \frac{\pi r}{6f}\left\{\frac{3}{2} - \frac{2}{z}\right\} \qquad [1]$$

where R is the grain radius for which particle pinning remains effective, r is the radius of the pinning particles, f is the volume fraction of the pinning particles, and z is a grain size heterogeneity factor.[2]

Changes in chemical composition (*e.g.* Ti or N levels), liquidus/solidus temperature, and cooling rate may influence the amount of TiN that may be precipitated in the solid and the temperatures over which precipitation occurs. Consequently, this study was designed to improve the fundamental understanding of TiN technology in steels produced *via* thin-slab casting. Titanium nitride particle size distributions and coarsening kinetics are examined in 0.05C, 1.2Mn steels with different Ti:N ratios to characterize their response to thin-slab casting. Some processing effects on precipitate evolution are also considered.

II. EXPERIMENTAL PROCEDURE

Eight commercial thin-slab cast steels were obtained for examination, along with one 25.4-cm-thick, conventionally cast (thick-slab) titanium-bearing steel for comparison. Systematic variations in titanium and nitrogen concentrations were intended in the thin-slab samples, and the resulting chemical compositions are summarized in Table I. The TiN ratios are provided in Table II. In this article, each steel is identified by its number indicated in Table I. The thin slabs were direct charged into a tunnel furnace after casting and allowed to equilibrate for 30 minutes at a temperature of about 1100 °C. The slabs then entered a five stand hot strip mill and were reduced from an initial slab thickness of approximately 50 mm to a sheet thickness between 4.32 and 8.69 mm (Table II). The finish rolling temperature was approximately 870 °C. The product was water spray cooled and coiled at approximately 635 °C before air cooling.

The Ti and N levels in the steels are plotted on a TiN solubility diagram in Figure 1. The diagram presents loci representing the various combinations of solute Ti and N in austenite, which are in equilibrium with TiN at different

MICHAEL T. NAGATA, former graduate (M.S.) student, JOHN G. SPEER, and DAVID K. MATLOCK, Professors, are with the Advanced Steel Processing and Products Research Center, Colorado School of Mines, Golden, CO 80401. Contact e-mail: jspeer@mines.edu

Manuscript submitted January 25, 2002.

Table I. Chemical Composition (Product Analysis) of Steels

Steel Designation	Element (Wt Pct)												
	C	Mn	P	S	Si	Cu	Ni	Cr	Mo	V	Al	Ti	N
Thin-Slab Cast													
[1] 0.009Ti 0.014N	0.048	1.23	0.026	0.006	0.029	0.120	0.060	0.022	0.018	0.004	0.026	0.009	0.014
[2] 0.008Ti 0.009N	0.062	1.20	0.018	0.006	0.020	0.094	0.048	0.022	0.014	0.003	0.026	0.008	0.009
[3] 0.048Ti 0.008N	0.048	1.37	0.005	0.005	0.007	0.090	0.044	0.026	0.015	0.005	0.021	0.048	0.008
[4] 0.022Ti 0.016N	0.049	1.20	0.011	0.002	0.028	0.100	0.050	0.027	0.010	0.004	0.023	0.022	0.016
[5] 0.021Ti 0.013N	0.056	1.19	0.014	0.003	0.018	0.093	0.050	0.020	0.012	0.004	0.021	0.021	0.013
[6] 0.011Ti 0.009N	0.053	1.16	0.011	0.003	0.030	0.099	0.043	0.023	0.012	0.003	0.020	0.011	0.009
[7] 0.014Ti 0.013N	0.056	1.16	0.020	0.007	0.010	0.096	0.045	0.016	0.014	0.003	0.024	0.014	0.013
[8] 0.022Ti 0.007N	0.046	1.23	0.006	0.003	0.012	0.090	—	0.045	0.013	0.005	0.022	0.022	0.007
Conventionally Cast													
[10] 0.015Ti, 0.006N	0.089	1.24	0.002	0.008	0.240	0.012	0.009	0.028	0.007	0.018	0.034	0.015	0.006

Table II. Ti:N Ratio, Solubility Temperatures Using $[Ti]_\gamma[N]_\gamma = 0^{((-8000/T\text{K})+0.32)}$ (3), and As-Rolled Sheet Thickness for Experimental Steels

Steel Designation	Ti:N Ratio Stoichiometric = 3.41	$T_{\text{Solubility}}$ (°C)	As-Rolled Thickness (mm)
Thin-Slab Cast			
[1] 0.009Ti 0.014N	0.64	1623	8.69
[2] 0.008Ti 0.009N	0.89	1522	4.32
[3] 0.048Ti 0.008N	6.00	1875	5.77
[4] 0.022Ti 0.016N	1.38	1847	5.94
[5] 0.021Ti 0.013N	1.62	1787	5.82
[6] 0.011Ti 0.009N	1.22	1577	4.34
[7] 0.014Ti 0.013N	1.08	1697	—
[8] 0.022Ti 0.007N	3.14	1663	—
Conventionally Cast			
[10] 0.015Ti, 0.006N	2.50	1580	—

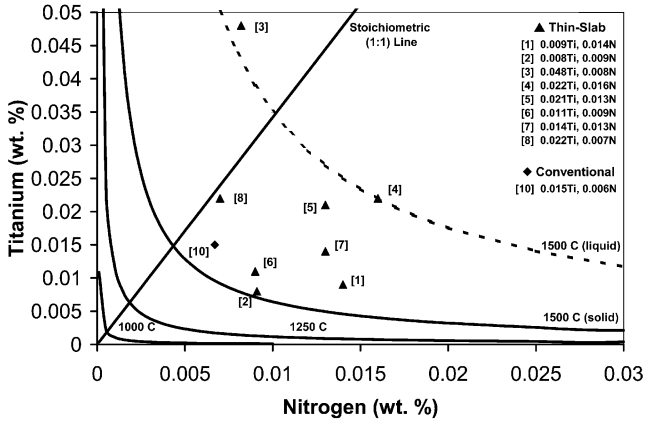

Fig. 1—Solubility plot showing chemical compositions of steels received for investigation.

temperatures. The steels were designed to have the TiN precipitates form in the solid state. The TiN solubility isotherms for liquid (dashed line) and solid (solid line) are shown in Figure 1 for 1500 °C, a temperature approximately where both solid and liquid steel may coexist. When the Ti and N levels fall below the 1500 °C liquid line and above the 1500 °C solid line, as they essentially do for the steels in this study, TiN precipitation is expected to begin at high temperature after solidification. Solubility isotherms are also shown for temperatures of 1250 °C and 1000 °C, for reference. The temperature at which TiN particles can begin to precipitate was calculated and is shown in Table II (*i.e.*, the solution temperature). A hyperstoichiometric steel (designated as steel [3] in Table I) was received, which could be compared to a hypostoichiometric steel (steel [4]) along a similar solubility isotherm in Figure 1, thereby having a similar driving force for precipitation. Steels with similar solution temperatures should have comparable driving forces for precipitation. A steel with a near-stoichiometric Ti:N ratio (steel [8]), which could be compared with a hypostoichiometric steel (steel [1]) of similar driving force, was also obtained. Driving force differences could be studied with several of the excess nitrogen steels for which the Ti and N levels nearly fall on a line parallel to the "stoichiometric" line indicated in the figure. For example, steels [5] and [6] can be compared to examine driving force differences. In this instance, the supersaturation at a given temperature could be greater for steel [5], with higher Ti and N levels, and greater precipitate volume fractions are consequently expected at equilibrium. However, the equilibrium solute concentrations after precipitation are identical for steel compositions falling on a line parallel to the stoichiometric line. Equilibrium solute-Ti levels may also be influenced, *e.g.*, by changing Ti independent of the N, or for different compositions on a single solubility isotherm. Varying levels of Ti in solution upon cooling could have dramatic effects on mechanisms such as TiN coarsening.

Samples were taken at three points in the process at Nucor Steel (not all sample locations were available for all steels). A schematic illustration of the process, showing sampling points, *i.e.*, as-cast, equilibrated prior to rolling ("after-furnace"), and end product, is given in Figure 2.

The TiN precipitate dispersions were characterized by transmission electron microscopy of extraction replicas. The as-received materials in the cast and hot-rolled conditions were sectioned parallel to the rolling direction and mounted for metallographic preparation. The samples were mechanically ground and subsequently polished down to 0.25 μm using a diamond polishing compound. Prior to etching, each sample was cleaned with ultrasonic agitation. The surface was etched for 15 seconds using a 2 pct nital solution. Carbon was sputtered onto the samples for replication; then, the

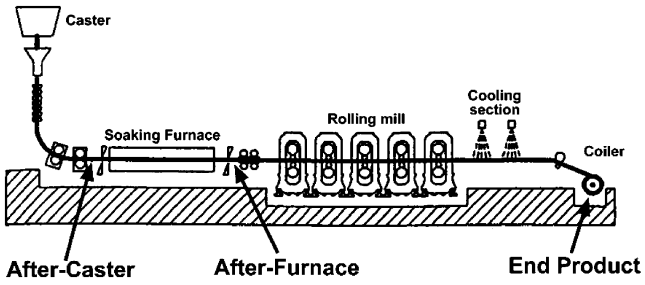

Fig. 2—Schematic of sampling locations in thin-slab casting process (courtesy of Korchynsky, used with permission[3]).

carbon layer was scribed into small squares to facilitate removal from the steel surface. Using a 5 pct nital solution, the carbon film was stripped from the specimens, releasing the precipitates along with the carbon. The carbon films were transferred to a solution of 50 pct deionized water and 50 pct methanol to remove the nital solution. They were then moved to a deionized water bath containing a small amount of methanol to reduce the surface tension. This bath uncurled the films so that they lay flat for removal from the solution with a copper grid.

The carbon replicas were examined using a PHILIPS* CM200 scanning transmission electron microscope (STEM). Particle sizes were measured as edge lengths of the cuboidal particles from TEM photomicrographs. A minimum of 50 particles were measured in each condition. Samples were taken from near the surface and centerline in the slab samples in order to determine cooling rate effects on precipitate size within a slab sample. Because of its reduced thickness, the final rolled product condition was examined without distinguishing surface and centerline regions.

*PHILIPS is a trademark of Philips Electronic Instruments Corp., Mahwah, NJ.

Particles from the centerline location of the slab samples were used for comparison, unless otherwise noted, recognizing that centerline samples might show the greatest coarsening due to the slower cooling rate. A Tukey–Kramer analysis[5,6,7] was used to make a rigorous statistical comparison between mean particle sizes of different steels. For comparisons between precipitates found at the surface and centerline, a *t*-test was used because only a single pair of results needed to be compared at one time.[8] A 95 pct confidence interval about the mean particle size was also determined for each condition, so that the results could be represented graphically here.

III. RESULTS

A. *Effects of Steel Composition*

1. *As-cast condition*

Samples from four of the steels were available in the as-cast condition. The TiN precipitate size data are presented in Figure 3 and indicate that the as-cast precipitate sizes of steels [1] 0.009Ti, 0.014N, [2] 0.008Ti, 0.009N, and [7] 0.014Ti, 0.013N are statistically indistinguishable from one another. Steel [8] 0.022Ti, 0.007N, however, contains slightly larger TiN particles than the others in the as-cast

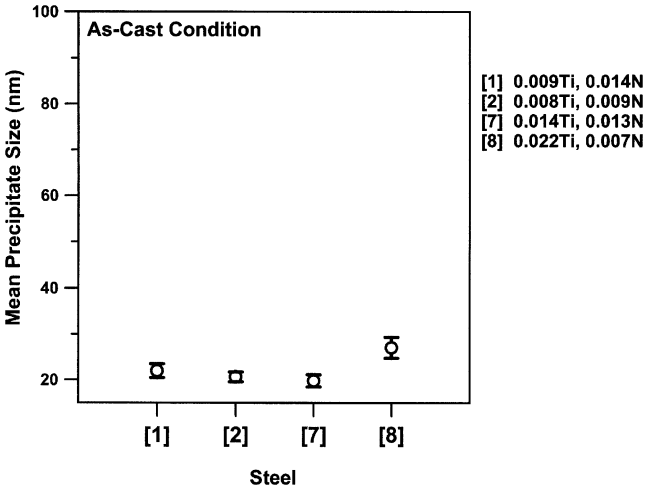

Fig. 3—Mean TiN particle size and 95 pct confidence interval for as-cast samples.

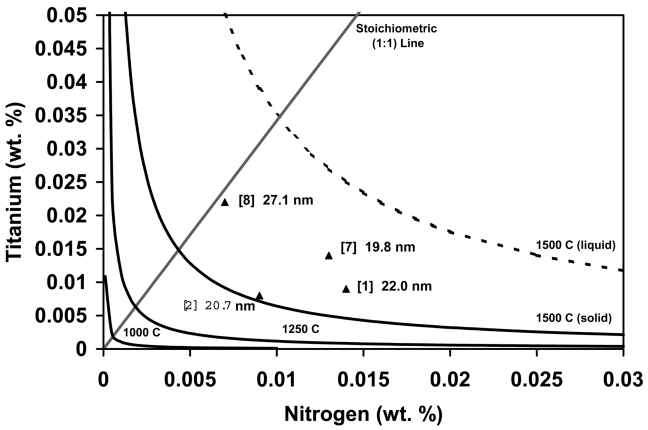

Fig. 4—TiN solubility diagram with mean particle sizes for as-cast samples.

condition, possibly due to its near-stoichiometric composition, indicated in the TiN solubility diagram in Figure 4. Near-stoichiometric compositions have been shown in previous studies on conventionally cast slabs to result in increased TiN particle sizes.[9] The titanium nitride particles are believed to increase in size due to Ostwald ripening during postsolidification cooling. The Wagner equation describes the kinetics of particle coarsening:

$$r_t^3 - r_0^3 = \frac{8\sigma D[\mathrm{Ti}]V}{9RT} \cdot t \qquad [2]$$

where r_t is the particle radius at time t, r_0 is the initial particle radius, σ is the particle/matrix interfacial surface energy, D is the diffusivity of the rate controlling specie (titanium) in the austenite matrix, [Ti] is the concentration of titanium in the matrix, V is the particle molar volume, R is the universal gas constant, and T is the temperature in Kelvin.[1] The Wagner equation is used to show that the TiN particle coarsening rate will be reduced in proportion to the decrease in titanium remaining in solution after precipitation.

2. *After-furnace condition*

Seven steels, [1] through [7], were sampled in the after-furnace condition, *i.e.*, after casting and then direct charging

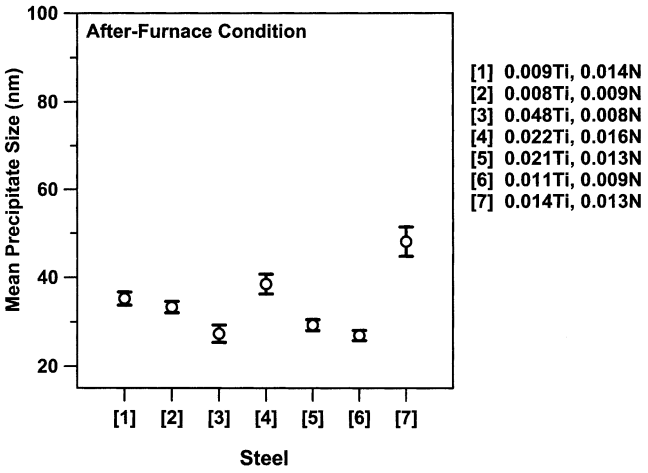

Fig. 5—Mean TiN particle size and 95 pct confidence interval for after-furnace sample.

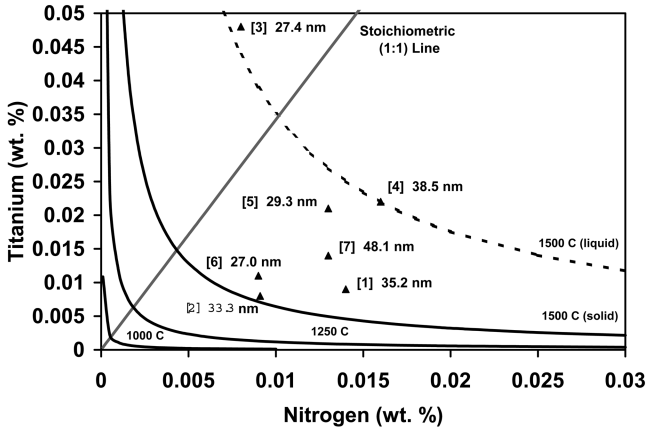

Fig. 6—TiN solubility diagram with mean particle sizes for after-furnace samples.

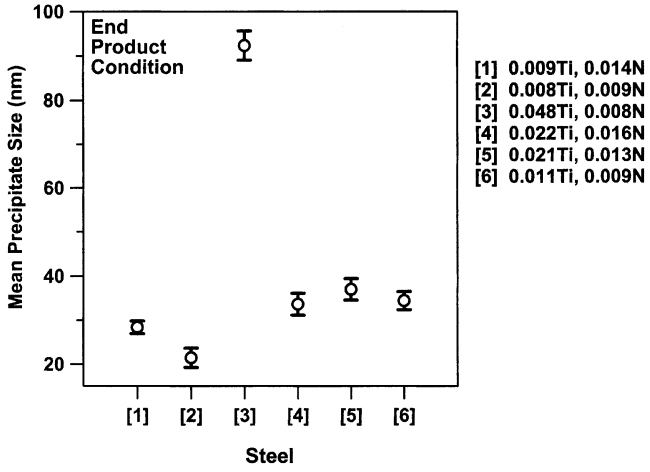

Fig. 7—Mean TiN particle size and 95 pct confidence interval for end product samples.

into a furnace and soaking ~30 minutes at 1100 °C prior to rolling. The precipitate size data in Figure 5 show that steels [3] 0.048Ti, 0.008N, [5] 0.021Ti, 0.013N, and [6] 0.011Ti, 0.009N have slightly finer mean TiN particle sizes than the other four steels. The Tukey–Kramer analysis indicated that TiN particle sizes in steels [2] 0.008Ti, 0.009N and [4] 0.022Ti, 0.016N are statistically different, although both are individually similar to steel [1] 0.009Ti, 0.014N. The TiN particles in steel [7] were somewhat coarser than in the other steels. While some clear differences in TiN sizes are indicated, it should be recognized that these differences were not large and the overall variation of mean particle sizes was within a factor of 2 for all steels examined here. The mean particle sizes were smaller than 50 nm, a value that has been suggested to be an effective size for austenite grain boundary pinning.[1] The seven different steel compositions are associated with different driving forces for precipitation, different Ti-solute concentrations, and different equilibrium volume fractions of TiN. These factors were carefully examined in an effort to explain the differences shown in Figure 5, although a unifying explanation that accounts for the average TiN particle size in every steel relative to each of the others was not apparent. Some possible effects may be considered, however. For example, steel [2] has the smallest driving force for precipitation during cooling, since it would fall on a solubility isotherm closest to the origin of Figure 6. This could suppress nucleation, leading to the presence of a smaller number of TiN particles having a larger size. The particles in steel [4] would correspondingly precipitate at a higher temperature than the other hypostoichiometric steels according to the solubility diagram in Figure 6. The TiN might form at or near the solidification temperature of this steel. Due to the increased diffusion rates at high temperatures, which assist growth and coarsening, larger particles may be present. It is believed that TiN precipitation occurred in the solid state in the materials used in this study, based on solubility considerations and the absence of precipitates with a dendritic appearance.

Steel [7] 0.014Ti, 0.013N appears to contain coarser TiN than all of the other steels. The reason for this behavior is not clear. Processing data (*e.g.*, furnace temperatures) were reviewed to determine whether this steel was exposed to higher soak temperatures, but the available data did not explain this behavior.

In light of conventional TiN alloying approaches, where hyperstoichiometric Ti:N ratios are not employed because of particle coarsening considerations,[8] the relatively fine precipitates found in steel [3] are noteworthy and their behavior will be addressed further in Section IV. Similarly, a clear effect of solute-Ti on coarsening is not apparent in the hypostoichiometric compositions. For example, steels [2], [5], and [6] have greater Ti:N ratios than steels [4], [7], and [1], but have smaller average TiN sizes despite the greater solute titanium concentrations expected at equilibrium.

3. *End product condition*

For the end product in the hot-rolled and coil-cooled condition, samples of six of the steels were available. The TiN particle sizes are shown in Figure 7. This section presents TiN size results based solely on Ti and N differences; the combined effects of rolling and chemical composition are considered further in the discussion. Differences between TiN precipitates in the hypostoichiometric steels were found to be small, as with the after-furnace condition. Nonetheless, some composition effects are apparent. Steel [2] 0.008Ti,

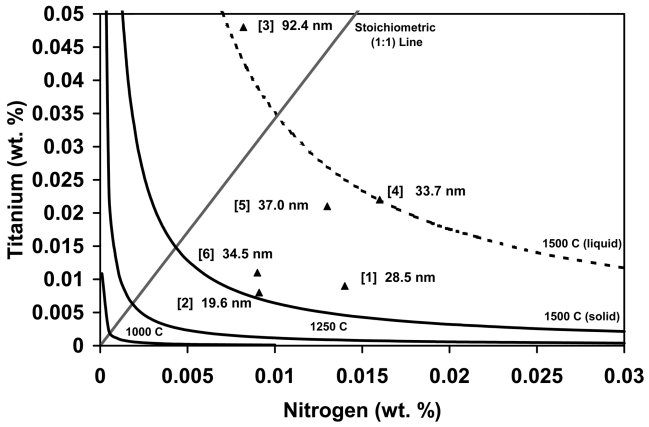

Fig. 8—TiN solubility diagram with mean particle sizes for end product samples.

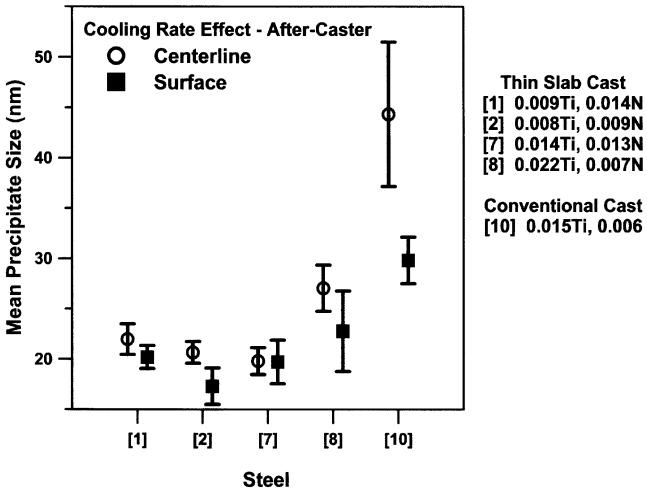

Fig. 9—Mean TiN particle size and 95 pct confidence interval at centerline of the after-caster slab product for thin-slab steels and thick-slab cast steel [10].

0.009N, with the finest particle size, is similar only to steel [1] 0.009Ti, 0.014N. The solubility diagram in Figure 8 shows that steel [2] has the highest solubility, which gives it the lowest driving force. Low driving force may result in precipitation at lower temperatures during cooling, resulting in smaller particles. It should be noted that low driving forces can also suppress nucleation at a given (*e.g.*, elevated) temperature and result in a greater particle size for precipitation at that temperature, so the potential effects of driving force may be complex. For example, the low driving force for steel [2] was previously associated with coarser particles in the after-furnace condition. The reversal in this trend for the final product sample points out the importance of chemistry/processing interactions, which will be discussed further subsequently.

The average TiN particle size in steel [1] is also statistically equivalent to the average size in steels [4] 0.022Ti, 0.016N and [6] 0.011Ti, 0.009N. Steel [5] 0.021Ti, 0.013N is also equivalent to steels [4] and [6]. The solubility diagram in Figure 8 includes the average particle sizes for the different steels. The figure shows that steel [6] and steel [5] have relatively similar precipitate sizes, as do steels [1] and [4]. Each steel pair defines a line that is essentially parallel to the stoichiometric line, as mentioned previously. Perhaps as excess nitrogen content is increased from steels [5] and [6] to steels [1] and [4], the particle size decreases slightly. In support of this potential excess-N effect, Zajac *et al.*[10] state that the volume fraction of fine nitrides remaining at higher temperatures would increase with enhanced nitrogen in the hypostoichiometric region, due to the reduced coarsening associated with a decrease in solute titanium.

The most significant result in Figure 7 is the very large TiN precipitate size in steel [3] 0.048Ti, 0.008N for the end product condition. The previously described Wagner equation indicates that the TiN particle coarsening rate will be increased in proportion to the amount of titanium left in solution. Thus, the excess-Ti steel [3] 0.048Ti, 0.008N has the potential for extensive coarsening. As mentioned previously, the greatest particle coarsening for this hyperstoichiometric steel was expected to be found after the soaking furnace, so it was somewhat surprising to find much larger precipitates in the end product than in the after-furnace condition in light of the lower temperature and shorter times associated with hot rolling. The behavior of steel [3], including the role of processing (*i.e.*, rolling), is discussed in more detail later.

Summarizing the overall effects of steel composition on TiN size, it is clear that there are some significant effects that may relate to differences in driving force, solute level, *etc.* The effects are relatively small in most instances, although a substantially increased mean precipitate size was observed in the hot-rolled steel containing excess titanium. The differences between steel types were not constant when compared at different stages during processing, and thus, interactions between chemistry and processing appear to be important. These interactions are addressed in the discussion focusing on the role of downstream processing such as the soaking furnace and hot-rolling mill.

B. *Cooling-Rate Effects*

1. *After-caster*

Steels [1] 0.009Ti, 0.014N, [2] 0.008Ti, 0.009N, [7] 0.014Ti, 0.013N, and [8] 0.022Ti, 0.007N were sampled before the tunnel furnace, at the surface and center locations in the thin-cast slab. Similar results were obtained from a thick-slab sample produced at a different facility, steel [10] 0.015Ti, 0.006N, in order to compare thin-slab and conventional continuous casting processes. Despite likely differences in cooling rate, the resulting differences in TiN particle size between the surface and the centerline in the thin-slab cast steels were small, with steel [2] being the only one where any statistical difference was found with the *t*-test (also shown graphically in Figure 9 *via* comparisons of the confidence intervals). Figure 10 shows examples of TiN precipitates found at the surface and the centerline of steel [2], illustrating the similarity in precipitate size distributions. The small difference observed between steel [8] and the others was explained earlier as an effect of chemical composition associated with the increased coarsening kinetics when more Ti is left in solution in a near-stoichiometric composition. Cooling rate differences between thin-slab cast and conventional continuous cast samples are reflected in the shift of TiN particle sizes from both the center and surface locations.

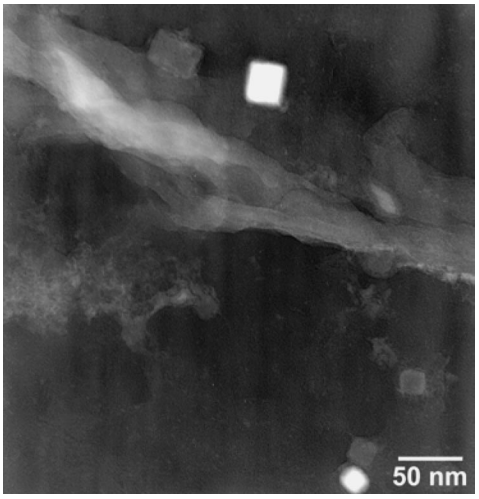

(*a*)

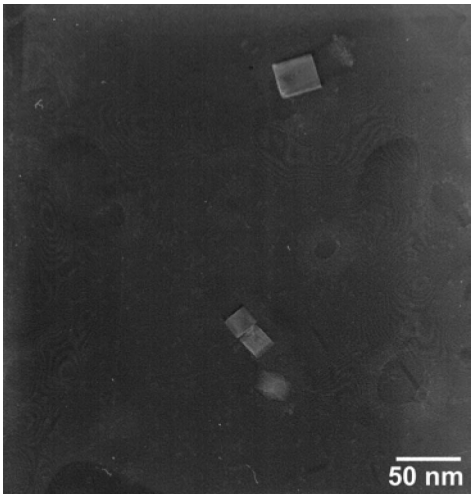

(*b*)

Fig. 10—Photomicrographs of TiN precipitates in steel [2] from after-caster condition (STEM): (*a*) centerline and (*b*) surface.

2. *After-furnace*

There of the steels ([1], [2], and [7]) examined in the as-cast condition were also examined in the after-furnace condition. The results for the after-furnace samples, shown in Figure 11, exhibit a much greater difference between the surface and centerline than for the as-cast samples shown in Figure 9. In all cases, the centerline precipitates are coarser than those examined at the surface; a typical example is shown for steel [2] in Figure 12.

IV. DISCUSSION OF PROCESSING EFFECTS ON TiN PRECIPITATION, GROWTH, AND COARSENING

A. *Effects of Tunnel Furnace*

The after-furnace precipitates are consistently larger than those of the as-cast (after-caster) product. The change in size is quite noticeable, as shown in the comparison of Figure 13 for the centerline location. The soaking temperatures, around 1100 °C for these thin-slab steels, coupled with the soaking time in the furnace, apparently give the particles an

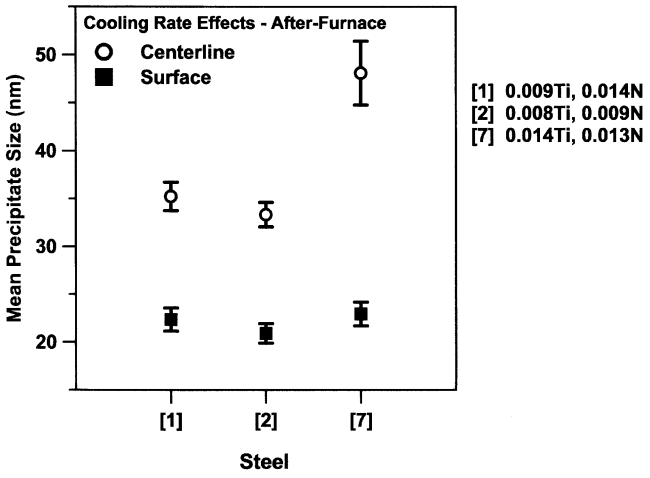

Fig. 11—Mean TiN particle size and 95 pct confidence interval for surface and centerline of after-furnace slab conditions.

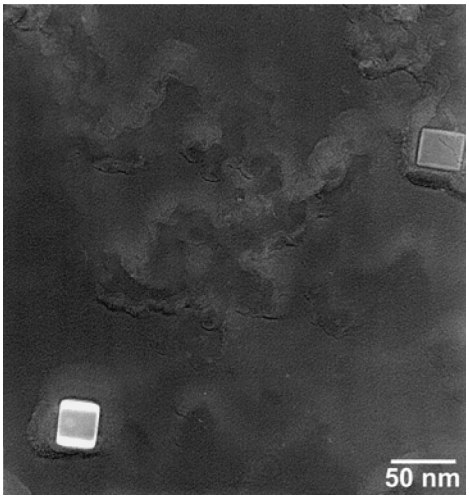

(*a*)

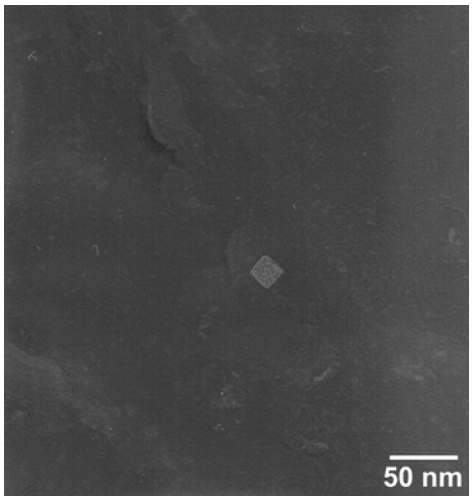

(*b*)

Fig. 12—Photomicrographs of TiN precipitates in steel [2] from after-furnace condition (STEM): (*a*) centerline and (*b*) surface.

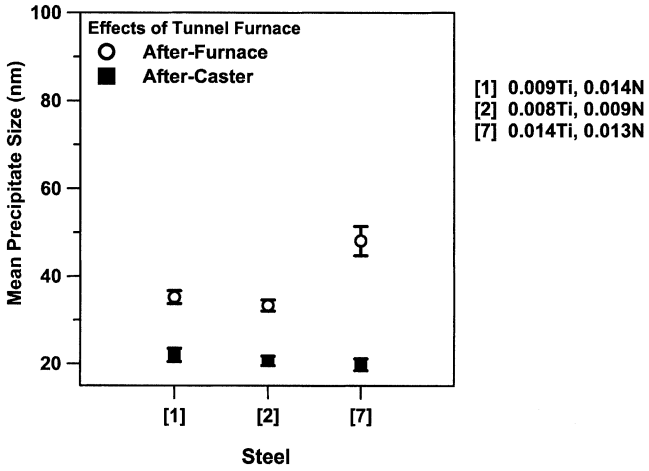

Fig. 13—Mean TiN particle size and 95 pct confidence interval at centerline of after-caster and after-furnace slab products.

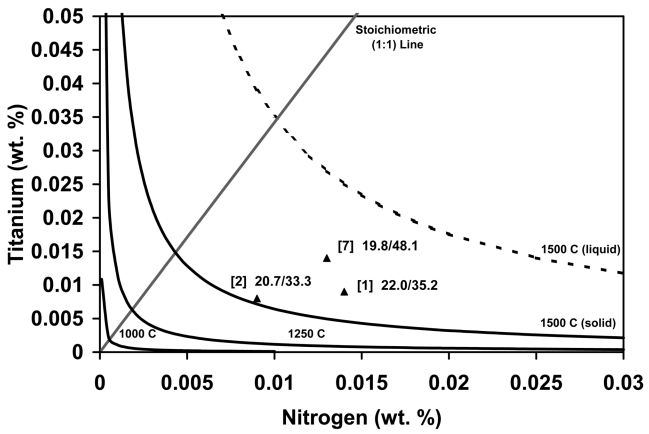

Fig. 14—TiN solubility diagram comparing mean particle sizes for after-caster and after-furnace conditions. The two numbers following steel designation number represent mean TiN particle sizes in nanometers. The first number is for the after-caster condition, and the second number is for the after-furnace condition.

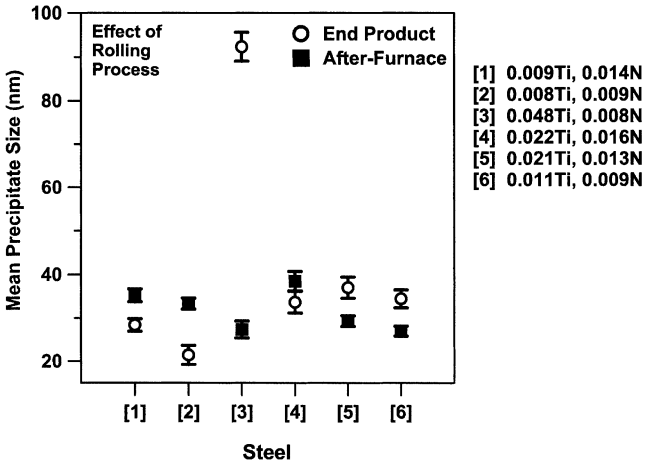

Fig. 15—Mean TiN particle size and 95 pct confidence interval of end product and after-furnace slab condition (centerline).

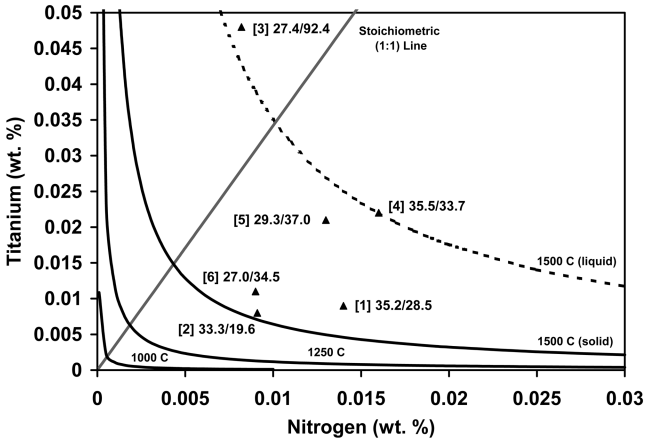

Fig. 16—TiN solubility diagram comparing mean particle sizes for end product and after-furnace samples. The two numbers following the steel designation number represent mean TiN particle sizes in nanometers. The first number is for the after-furnace condition, and the second number is for the end product condition.

environment conducive to further coarsening. The differences in particle size between the steels are presumably due to changes in Ti and N concentrations, since the time and temperature were similar between the steels. Consequently, the TiN particle size results are also shown in the solubility diagram for these three steels in Figure 14. The particles in steel [2], with the lowest driving force for precipitation, and steel [1], with the least solute Ti upon cooling, exhibit nearly the same increase in particle size in the tunnel furnace. The titanium left in solution in steel [7] would fall between the values in the other two steels as it cooled along a path parallel to the stoichiometric line, and thus there is no reason to expect a noticeably higher coarsening rate in steel [7]. Nonetheless, the TiN particles in steel [7] are larger in the after-furnace condition. It is possible that the higher TiN volume fraction expected in steel [7] is responsible. That is, the precipitation process may be incomplete in the cast slab, and continued particle growth may be greater in steel [7] due to the increased fraction of TiN expected. It should be noted that the volume fraction of precipitates is not accurately available from extraction replicas, and so particle growth associated with increasing total volume fraction (distinct from coarsening) during tunnel furnace soaking is difficult to assess quantitatively from these results.

B. *Effects of Rolling Process*

As mentioned earlier, the samples from the end product were taken without differentiating between centerline and surface due to reduced cross-sectional area (the sheet thickness being similar to the TEM specimen size). The end product data could be slightly skewed as a consequence, toward a smaller particle size when compared to the centerline data. That is, some small differences reported in particle size may be due to differences in the region of origin on the cross section in the end product sample. The TiN size results are shown in Figure 15 and plotted on a solubility diagram in Figure 16, comparing the end product and after furnace conditions for the six steels available in both conditions. This comparison should identify changes in the TiN size distribution occurring during or after the rolling process. Titanium nitride precipitates in the after-furnace and

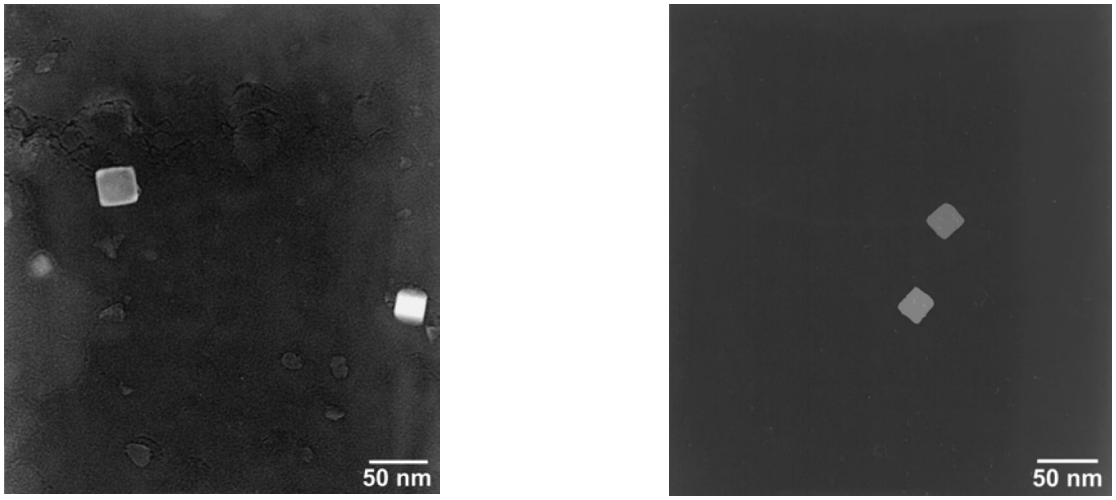

(*a*) (*b*)

Fig. 17—Photomicrographs of TiN precipitates in steel [1] 0.009Ti, 0.014N (STEM): (*a*) after-furnace (centerline) and (*b*) end product.

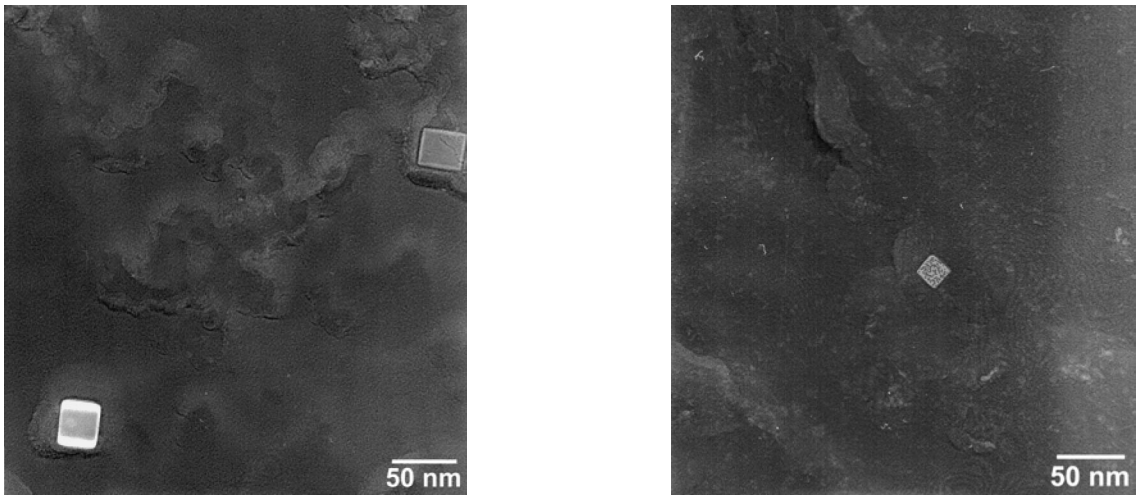

(*a*) (*b*)

Fig. 18—Photomicrographs of TiN precipitates in steel [2] 0.008Ti, 0.009N (STEM): (*a*) after-furnace (centerline) and (*b*) end product.

end product conditions are shown in Figures 17 through 21. The high-Ti hyperstoichiometric steel, steel [3], exhibits dramatic coarsening in the end product compared to the other steels, which are hypostoichiometric, or have excess nitrogen. There are also some small changes apparent in particle size within the excess nitrogen group of steels. It is particularly noteworthy that the titanium nitride precipitates in steel [2], with the smallest driving force for precipitation, and steels [1] and [4], with the most excess nitrogen, are on average slightly finer in the end product compared to the after-furnace condition.

In a study by Peterson *et al.*,[11,12] based on conventionally cast slabs, it was reported that precipitation of TiN in undeformed austenite is slow and that hot direct-rolled samples have a higher proportion of titanium remaining in solution at the onset of rolling, compared to cold-charged slabs. That is, as the schematic particle size distributions of Peterson *et al.* in Figure 22 suggest, much of the titanium may precipitate as a fine dispersion after rolling begins, compared to a coarser dispersion existing after reheating in the cold-charged material. The formation of new particles thus may result in apparent refinement of the precipitates. Perhaps the low driving force associated with steels [1] and [2] results in less precipitation before rolling, leaving more Ti in solution at the onset of rolling, and consequently formation of fine particles during rolling and thus a finer average particle size. It is well known that nucleation is enhanced by deformation (*e.g.*, reference 13), which may contribute to this mechanism of precipitate "refinement."

The other three steels, steel [3], with excess titanium, and steels [5] and [6], exhibit growth or coarsening between the after-furnace condition and the end product, *i.e.*, during rolling. Ostwald ripening is a well-documented mechanism by which large particles coarsen at the expense of the smaller particles,[14] whereby the number of particles decreases and the mean radius increases. The higher concentration of Ti left in solution upon cooling in steels [5] and [6] compared, *e.g.*, to steels [1] and [4] may facilitate the Ostwald ripening process, as discussed previously. For

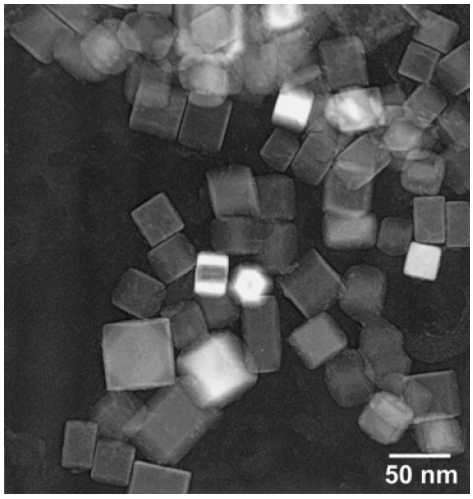

(*a*)

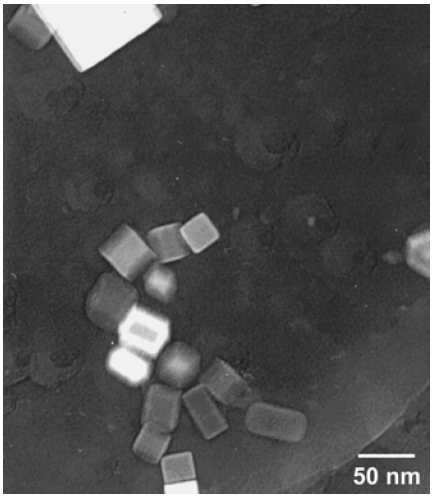

(*b*)

Fig. 19—Photomicrographs of TiN precipitates in steel [4] 0.022Ti, 0.016N (STEM): (*a*) after-furnace (centerline) and (*b*) end product.

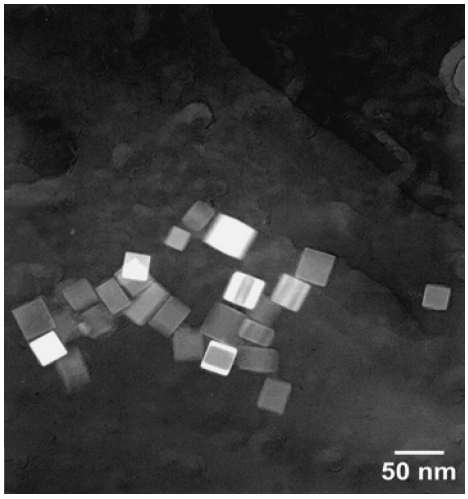

(*a*)

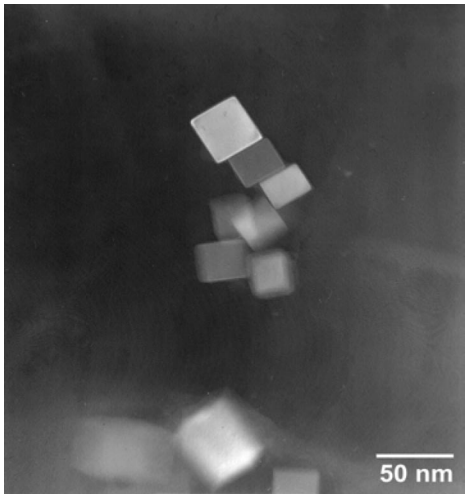

(*b*)

Fig. 20—Photomicrographs of TiN precipitates in steel [5] 0.021Ti, 0.013N (STEM): (*a*) after-furnace (centerline) and (*b*) end product.

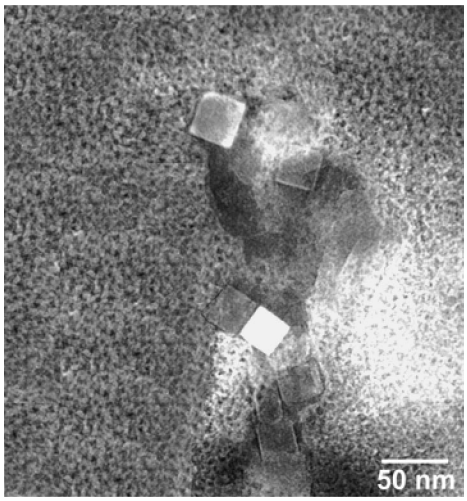

(*a*)

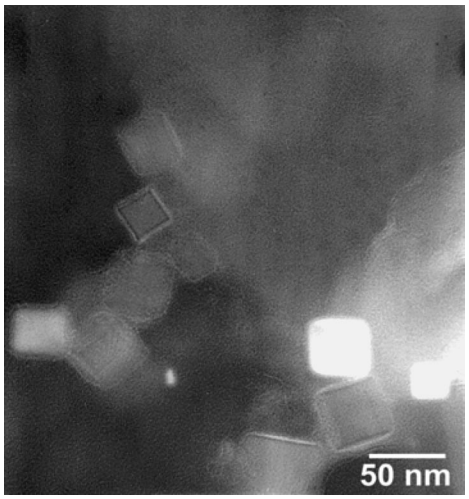

(*b*)

Fig. 21—Photomicrographs of TiN precipitates in steel [6] 0.011Ti, 0.009N (STEM): (*a*) after-furnace (centerline) and (*b*) end product.

steel [3], growth or coarsening during the rolling process was especially pronounced, as illustrated by the typical TiN precipitates shown in Figure 23. This steel is hyperstoichiometric (excess Ti), which means a much larger amount of titanium would be left in solution in the solid state, increasing the coarsening kinetics. While coarse TiN in this steel was considered possible because of the excess Ti, it was surprising that the dramatic increase in particle size occurred during rolling, rather than during casting or soaking in the tunnel furnace. The contribution of TiC precipitation at low temperature to the observed particle size is another consideration. Since the carbon concentration in the precipitates cannot be measured using the carbon-based replication technique chosen for this project, the possibility of increased precipitate size by epitaxial TiC formation on pre-existing TiN cannot be ruled out.

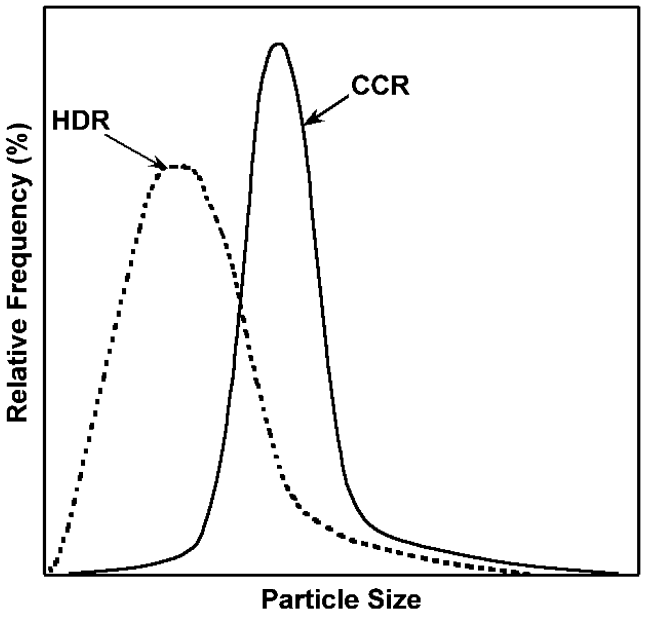

Fig. 22—Particle size distributions showing cold charge rolling (CCR) and hot direct rolling (HDR) (adapted from Ref. 14).

(The corners of the cuboidal TiN precipitates also appeared to be slightly more rounded in this steel, perhaps associated with the greater particle size or different precipitate composition.) Finally, a portion of the increase of particle size in steel [3] may be associated with completion of precipitation during rolling (*i.e.*, increasing volume fraction), as discussed previously.

Thermodynamic driving force for precipitation is related to two closely connected factors, the degree of undercooling (ΔT) or, equivalently, the supersaturation of solute Ti and N in the matrix. Larger driving forces would thus be expected at large undercoolings or high supersaturations.[15] In light of the study by Peterson *et al.* indicating that precipitation may be incomplete prior to rolling, the driving force associated with a higher proportion of titanium remaining in solution at the onset of rolling may be higher than previously believed and is perhaps even more important for thin-slab material due to the inherently fast cooling. This driving force may allow for growth of particles present after reheating, and an associated increase in particle size of the Ti-nitrides or carbonitrides, or, alternatively, nucleation of new particles, possibly leading to a decrease in average particle size.

Diffusivity of titanium, the rate limiting process, must be adequate for the TiN precipitates to grow or coarsen. Deviations from normal particle coarsening rates caused by diffusion "short circuits" such as dislocations and grain boundaries may also be important.[16,17] This increase in atom mobility due to the presence of defects allows more rapid Ostwald ripening of the already existing particles.[12] In the present work, the rolling deformation would increase dislocation densities, assisting the diffusion mechanism described previously. Deformation could also move jog-dragging screw dislocations, forming a line of vacancies through the matrix, which accelerate bulk diffusion, again aiding in Ostwald ripening. While "deformation enhanced coarsening" does not appear to be well documented in the literature, it remains a possible mechanism contributing to the dramatic increase in particle size after rolling observed in steel [3]. Evidence of diffusion along dislocations and grain boundaries has been well documented in

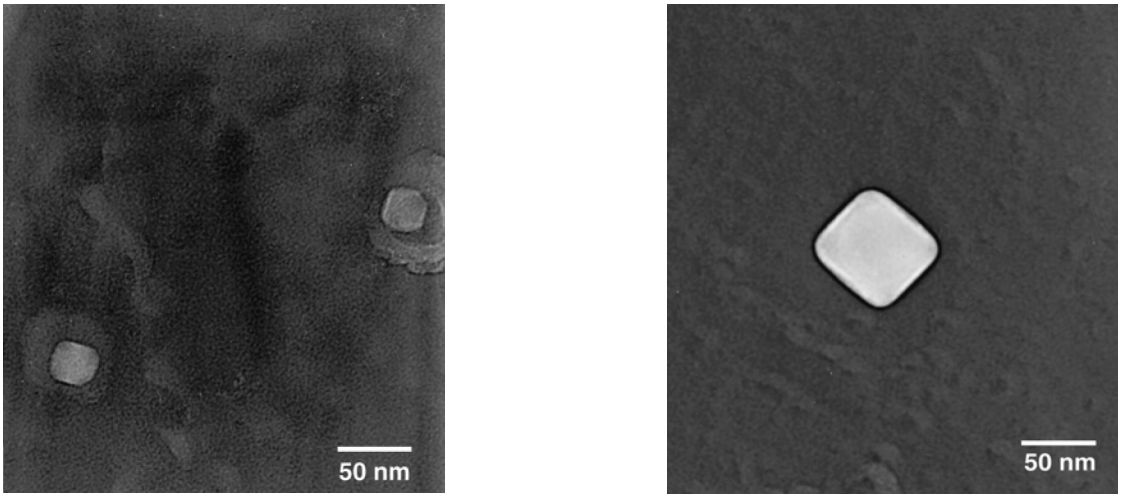

(*a*) (*b*)

Fig. 23—Photomicrographs of TiN precipitates in the hyperstoichiometric steel [3] (STEM): (*a*) after-furnace (centerline) and (*b*) end product.

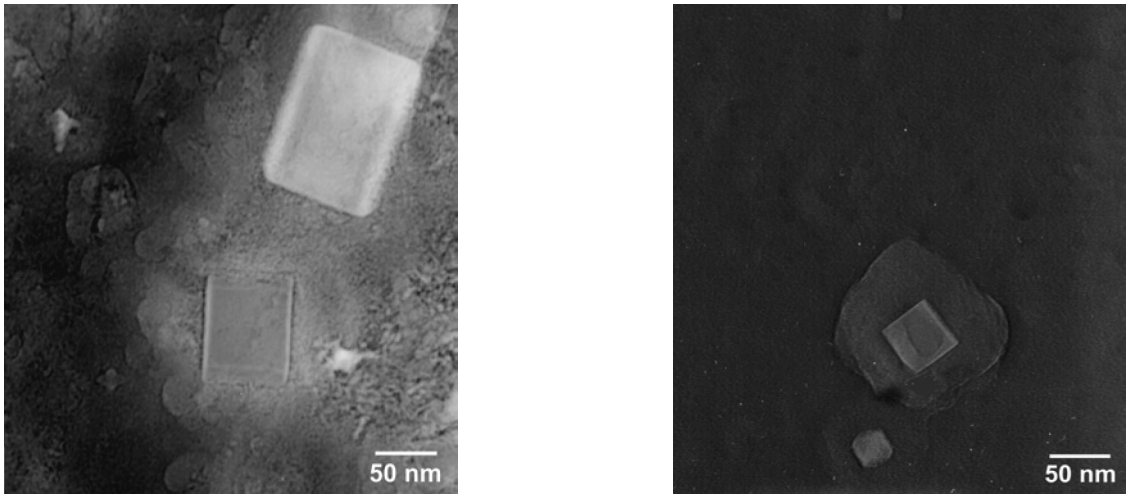

(*a*) (*b*)

Fig. 24—Photomicrographs of TiN precipitates in the conventional cast steel [10] (STEM): (*a*) centerline and (*b*) surface.

work concerning increased diffusion in high-temperature deformation.[18]

C. *Cooling-Rate Effects*

The precipitate data taken at the surface and at the centerline in several thin-slab cast steels, and the conventional-cast thick slab, facilitated examination of cooling rate effects on precipitate size. There are several interesting points found in the as-cast data shown in Figure 9. There is a substantial difference in precipitate size between steel [10], the thick slab, and the other four steels, which were all thin slabs. The conventionally cast thick-slab TiN particles are larger in both the centerline and surface samples when compared to the thin-slab samples. With the slower solidification and postsolidification cooling rate of the thick-slab cast samples, an overall increase in TiN particle size is not surprising.[9] The centerline of the slab is generally at a higher temperature for a longer period of time, promoting growth and coarsening. Additionally, the slower solidification rate might also cause precipitates to form in the liquid rather than solid state, leading to greater particle sizes. Examples of particles found at the surface and centerline of the conventionally cast steel [10] are shown in Figure 24.

It is also noted that the confidence interval associated with the particle size measurements is wider for the thick-slab data, meaning there is greater variability of particle sizes. Several factors may contribute to this variability. With more time at temperature in the thicker slabs, nucleation may occur in over long periods of time; therefore, small particles that nucleate late in the process and larger particles that formed early in the process can both exist in the cast product. Wider distributions of precipitate sizes may occur early in the Ostwald ripening process, whereby some coarsened particles, as well as smaller particles that were beginning to decrease in size would both be present, contributing to particle size variation.[19] Finally, it is also recognized that differences in the chemical composition variations could also influence the particle size distributions.

V. CONCLUSIONS

1. Clear differences between TiN dispersions were observed in different thin-slab cast steels having variations in titanium and nitrogen concentrations. Many of these differences could be understood in terms of variations in driving force for precipitation and solute-Ti available during coarsening.
2. The TiN particle size decreased with increasing cooling rate, as expected. The TiN precipitates were larger in a conventional thick slab compared to the thin slabs and at the slab centerline in comparison to the near-surface. The surface/centerline differences were particularly greater in the conventionally cast thick slab.
3. The precipitates in the hyperstoichiometric (excess Ti) steel were fine after casting and soaking, but increased substantially in size between the after-furnace and end product conditions (*i.e.*, during rolling). A number of factors were thought to be relevant in explaining this observation, such as the solute Ti and remaining supersaturation, the increased defect density from deformation, and the resulting accelerated solute diffusion and associated precipitate coarsening.
4. The observed precipitate sizes suggested that TiN precipitation may be incomplete after thin slab casting, hot charging, and tunnel furnace soaking, consistent with earlier reports. Interactions between steel composition and processing were also important. For example, the average TiN size decreased in some steels during/after the final hot-rolling process, but increased in others. This behavior was believed to be associated with the competition between coarsening in some steels and completion of precipitation in others.

ACKNOWLEDGMENTS

This work was supported by the NSF through Award No. EEC-9812842 and by the sponsors of the Advanced Steel Processing and Products Research Center, an NSF Industry/University Cooperative Research Center. Lynn Ondrovic,

Nathan Fraser, and Donna Demark (Nucor Steel) and Richard Bodnar (Bethlehem Steel Corporation) are gratefully acknowledged for providing samples.

REFERENCES

1. R.L. Bodnar: *Iron Steelmaker*, 1994, vol. 21(4), pp. 19-24
2. W. Roberts: *HSLA Steels—Technology and Applications*, ASM, Metals Park, OH, 1984, pp. 33-65.
3. S. Matsuda and K. Okumura: *Trans. Iron Steel Inst. Jpn.*, 1978, vol. 18, p. 198.
4. M. Korchynsky and S. Zajac: *Proc. Int. Conf. on Thermomechanical Processing in Theory, Modeling and Practice*, Stockholm, Sweden, September 4-6, 1996, *Swedish Society for Materials Technology*, Stockholm, Sweden, 1997, pp. 369-81.
5. J. Klockars and G. Sax: *Sage University Paper Series on Quantitative Applications in the Social Sciences*, Sage, Newbury Park, CA, 1986.
6. L.E. Toothaker: *Sage University Paper series on Quantitative Applications in the Social Sciences*, Sage, Newbury Park, CA, 1993.
7. D. Schiff and R.B. D'Agostino: *Practical Engineering Statistics*, John Wiley & Sons, New York, NY, 1996.
8. M.T. Nagata: Master's Thesis, Colorado School of Mines, Golden, CO, June 2001.
9. F.B. Pickering: *Titanium Technology in Microalloyed Steels*, The Institute of Materials, London, 1997, pp. 10-43.
10. S. Zajac, R. Lagneborg, and T. Siwecki: *Proc. Int. Conf. "Microalloying '95,"* ISS, Warrendale, PA, 1995, pp. 321-38.
11. R.C. Peterson, B.A. Parker, and R.K. Gibbs: *Int. Symp. on Low-Carbon Steels for the 90s*, R. Asfahani and G. Tither, eds., TMS-AIME, Warrendale, PA, 1993, pp. 131-37.
12. R.K. Gibbs, R.C. Peterson, and B.A. Parker: *Proc. Int. Conf. on Processing, Microstructure and Properties of Microalloyed and Other Modern High Strength Low Alloy Steels, Iron and Steel Society*, Warrendale, PA, 1992, pp. 201-07.
13. G. Sauthoff: *J. Phys.*, 1996, vol. 6, pp. 87-97.
14. P.W. Voorhees: *Ann. Rev. Mater. Sci.*, 1992, vol. 22, pp. 197-215.
15. E.J. Palmiere: *Microalloying '95*, ISS, Warrendale, PA, 1995, pp. 307-20.
16. D.A. Porter and K.E. Easterling: *Phase Transformations in Metals and Alloys*, Chapman & Hall, London, 1992.
17. R.E. Reed-Hill and R. Abbaschian: *Physical Metallurgy Principles*, PSW Publishing Company, Boston, MA, 1994.
18. R.W. Hertzberg: *Deformation and Fracture Mechanics of Engineering Materials*, John Wiley & Sons, New York, NY, 1989.
19. S.C. Hardy and P.W. Voorhees: *Metall. Trans. A*, 1988, vol. 19A, pp. 2713-21.